Development and Verification of a Distributed Electro-Thermal Li-Ion Cell Model

Stocker, R., Lophitis, N. & Mumtaz, A.

DOI 10.1109/IECON.2018.8591633
ISSN 2577-1647

Publisher: IEEE

Development and Verification of a Distributed Electro-Thermal Li-Ion Cell Model

Richard Stocker[ab*], Neophytos Lophitis[a], Asim Mumtaz[c],
[a]Faculty of Environment, Engineering and Computing, Coventry University, Coventry, CV1 5FB, United Kingdom
[b]Controls and xEV group, HORIBA-MIRA, Nuneaton, CV10 0TU, United Kingdom
[c]Stephenson Institute for Renewable Energy, University of Liverpool, United Kingdom, L67 7ZF
*Corresponding author. Tel: +442476355275. Email Richard.Stocker@horiba-mira.com

Abstract-This paper presents a 1D distributed electro-thermal li-ion cell model. The model is intended to give accurate representation of cell thermal and electrical characteristics in response to current application, highlighting distributions of these parameters across the cell. It is also designed to be compact and fast simulating. A generalized parameterization approach allows the model to be easily adaptable to different cell designs and chemistries. The model achieves this by combining a thermal model based on thermal laws, with an electrical equivalent circuit model, both populated by empirical data accessible through simple individual cell testing. In this paper, the model is explained, and simulation results are correlated against a Nickel Manganese Cobalt (NMC)/graphite cell cycled under constant current and also dynamic conditions without cooling. It was found that the model provides accurate results when compared to a constant current discharge and representative drive test cycle.

Keywords: Lithium-ion, battery cell, simulation, model

I. Introduction

Electrical/hybrid vehicles are demonstrating a continual and accelerating growth of automotive market share [1]. With this comes the increased need for development and verification of robust, compact and effective battery packs, which are becoming significant vehicle components. A key aspect of any modern design/verification strategy is simulation, creating a need for accurate cell level models. These models may also be used for BMS development. In this work there has been the development of an electro-thermal cell model, which with its efficient, compact approach, can achieve fast simulation times while still achieving sufficiently accurate information about cell thermal/electrical characteristics and their distribution across cell thickness/diameter. It is designed to be easily adapted to different cell geometries and chemistries, through intelligent development of model parameters from of easily acquired test data. While there are many papers which model thermal [6]–[11] and electrical [9], [12], [13] distributions across a cell, are compact [14], [15], adaptable to different conditions [8], and optimized [9], there is room for developing a model that achieves all of these aspects. The model developed as described in this paper achieves these goals. This paper explains the model, and presents the results of a correlation exercise against constant current and dynamic cell discharge tests.

II. Model Rationale and Structure

The model has been designed to have all required parameters to estimate performance, and eventually to inform models on cell aging. A thermal model is included, as it has well known that cell internal temperatures impact available capacity[18]–[20], impedance [20], [21], and lifetime [11]. An electrical model is also developed, giving cell voltage as a function of cell energy and response to current. It also estimates State-of-Charge (SoC) and emulates its effects on cell characteristics such as
internal resistance [12]. Due to the strong interactions between the thermal and electrical characteristics of a cell, both models will be coupled in a closed loop, illustrated in Fig. 1.

An observed phenomena in large, energy dense cells, is that electrical and thermal conditions can vary throughout the cell thickness [3]–[6], [13], [14], which in extreme cases can lead to differences in lithiation across the active material 'jellyroll' [15], affecting cell performance and lifetime [5] [14]. To account for this, a 1D nodal distribution has been incorporated into the electrical and thermal models, with different possible interpretations dependent on cell geometry. For prismatic/pouch cells, the nodal distribution occurs along the thickness of the cell i.e. the direction in which the jelly roll components are stacked, as shown in Fig. 2. For cylindrical cells, the nodes are evenly spaced across the radial dimension, as shown in Fig. 3. For prismatic cells, nodes 1 and N have interactions with the surface, with other nodes interacting with each other. For cylindrical cells, the nodes are spaced in the radial direction, as shown in Fig. 4. Additional nodes are also used to represent the cell positive and negative terminals, which have conduction with all cell layers.

The model platform is Matlab/Simulink. This was chosen for its versatility in conditions such as sample time and solver selection, and its ability to allow implementation of a bespoke model construct, while still allowing for fast simulation times.

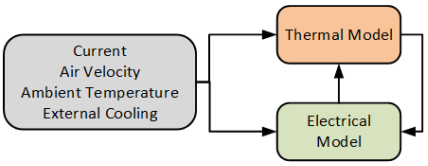

Fig. 1 Model interactions and interface

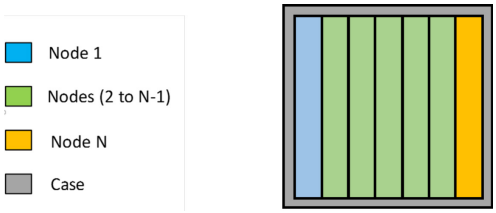

Fig. 2 Modal Nodal Structure Prismatic Cells

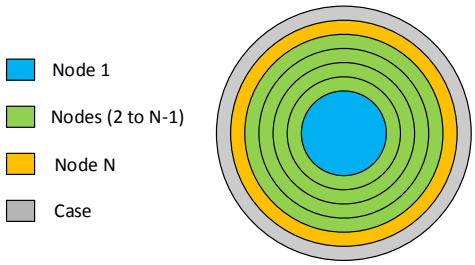

Fig. 3 Modal Nodal Structure Cylindrical Cells

III. Thermal Model

The thermal model contains temperature states for each node. It quantifies heat generation during each timestep, calculating heatflow both between nodes and between the cell model and the external system. It does this by taking in the relevant electrical and external inputs, as shown in Fig. 4, and applying the heat balance equation shown in (1).

(1) shows temperature distribution of active material, as a function of the 4 main contributions to thermal power transfer: irreversible heating $\dot{q}_{ir}$, reversible entropic power transfer $\dot{q}_e$, convection between the cell and environment $\dot{q}_c$ and power transfer due to external cooling $\dot{q}_{ex}$. Thermal power transfer is converted into temperature change via the cell mass and specific heat capacity. These characteristics are individual to each cell, and are taken from either manufacturer data or reliable literature sources [37], [38].

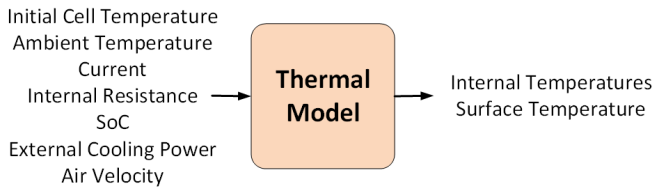

Fig. 4 Thermal Model Interfaces

Irreversible heat generation is due to inefficiencies resulting from lithium-ion cell resistance to charge transfer [16]. This can be modeled as the resistance dependent voltage deviation from open circuit voltage multiplied by applied current[4], [5], [10], [17], [18], commonly expressed as in (2).

There is also reversible thermal power transfer due to the phase changes that occur in cell active materials during cycling. This is dependent on cell temperature, applied current, and entropic coefficient, as shown in (3) [10], [13], [18]. The entropic coefficient is unique to each cell, and is usually empirically calculated by analysing the change in open circuit voltage with temperature across the usable capacity range [2], [3], [10], [16], [19]. This coefficient is typically linear with temperature, but varies with SoC [19].

An exposed cell cannot be treated in isolation, and thermally interacts with the external environment through convective effects, modelled by (4). This general equation has been used in models previously [3], [7], [16], [20]. This thermal transfer inherently affects the cell surface more than its center, which in some circumstances promote thermal gradients [21] [14].

Literature values of convection coefficients range considerably, suggesting a dependence on cell design and air flow characteristics [6], [38], [40], [45], [47], [48]. To account for this, the cell surface convection coefficient is modelled using known properties of air, taken from [23], and relations for natural and forced convections for either flat surfaces or cylinders, depending on cell geometry [8], [50]–[52].

The final term included in the heat balance is external cooling. This allows the simulation of power transfer from systems such as external thermal management systems, that could include mechanisms such as liquid cooling or phase change materials [4], [16], [18]. This power term is applied to either the cell surface or terminals, depending on the cooling method, and is also a consideration in thermal gradients [26].

To account for temperature distributions across the cell however, the above approach was expanded to a 1D nodal structure which could show thermal distribution across either the thickness (in the case of prismatic/pouch) or radial direction (cylindrical) cell direction. This direction was chosen due to the low thermal conductivity of the separator reducing thermal conductivity through jelly roll thickness, and due to thermal gradients being more significant to aging in this direction [14]. To correctly model the interactions between the jelly roll and external environment, additional nodes were added for the terminals and case.

$$m_{cell}Cp_{cell}(T_N-T_{N-1})=\dot{q}_{ir}+\dot{q}_{ex}-\dot{q}_c-\dot{q}_e \quad (1)$$

$$\dot{q}_{ir}=I^2R\ [W] \quad (2)$$

$$\dot{q}_e=T_{cell}\Delta S=-T_{cell}I\left(\frac{\delta V_{oc}}{\delta T}\right) \quad (3)$$

$$\dot{q}_c=h_sA_s(T_s-T_a) \quad (4)$$

IV. Electrical Model

An equivalent circuit approach was used for the electrical model due to its ease of parameterization for different cells, and quick computational speed. Equivalent circuit models for Li-ion cells are usually based on open circuit voltage input, and elements representing contributions to cell resistance. The resistance contributions of a new cell can be characterized into 3 effects: ohmic, charge transfer polarization and diffusion [24], [54]. Ohmic resistance is applied instantaneously from current application due to material resistance of cell components such as the electrolyte, electrode materials and terminals. Charge transfer polarization resistance results from the chemical reactions occurring on the electrode, and diffusion is due to the mass transport limitations of the

electrolyte and electrode materials [55], [56]. Ohmic resistance is typically modelled as a single resistor, with additional resistance components modelled as resistor-capacitor pairs.

A study of different equivalent circuit approaches found that the best compromise between accuracy and modelling efficiency was a resistor paired with one parallel connected resistor and capacitor [9]. In fitting to empirical data however, it was found by the authors that 2 RC curves gave much more representative emulation of real data than a single RC curve, as shown in Fig. 6. This led to the choice of equivalent circuit shown in Fig. 5. The resulting state and output equations are shown in (5) and (6).

$$\{\dot{x}\}=\begin{Bmatrix}\dot{V}_p\\ \dot{V}_d\end{Bmatrix}=\begin{bmatrix}\frac{-1}{R_p*C_p} & 0\\ 0 & \frac{-1}{R_d*C_d}\end{bmatrix}\begin{Bmatrix}V_p\\ V_d\end{Bmatrix}+\begin{Bmatrix}\frac{1}{Cp_t}\\ \frac{1}{Cd_t}\end{Bmatrix}I \tag{5}$$

$$\{y\}=\{V_T\}=[1 \quad 1]\begin{Bmatrix}V_p\\ V_d\end{Bmatrix}+R_oI+V_{oc} \tag{6}$$

Each model element required population over the known operating range. This took the place of empirical data, populated by an array of charge/discharge pulse testing at different temperature and current conditions, similar to that performed in [28]. Open circuit voltage (OCV) depends heavily on SoC, and has mild dependence on temperature [29]. There is a strong hysteresis effect of open circuit voltage based on current history [26][38] with true OCV only occurring after several hours [30]. To account for hysteresis, separate 2D OCV maps were implemented for charge and discharge.

Charge transfer and polarization resistance are heavily dependent on temperature, SoC, current direction[27], and current magnitude [31]. While ohmic resistance is independent of SoC [27], it is dependent on temperature [27], and in our data showed slight dependencies on SoC and current. Maps using these parameters were developed for all model elements.

SoC is an essential model state due to its influence on cell electrical and thermal behavior. It is modelled based on the commonly used coulomb counting algorithm [64]–[67], with the initial estimation using the OCV-SoC relationship under relaxed conditions [32], [33] which the cell is assumed to be at the simulation start.

It has been suggested that cell internal behaviour between cell layers, emulates that of full cells in parallel [12][68]. This approach was taken to model the distribution. The approach for modelling parallel cells was adapted from [34]. The resultant equations are shown in (7-13).

$$\begin{Bmatrix}\dot{x}_1\\ \dot{x}_2\\ \dot{x}_3\\ \vdots\end{Bmatrix}=\begin{bmatrix}A_1 & 0 & 0 & 0\\ 0 & A_2 & 0 & 0\\ 0 & 0 & A_3 & 0\\ 0 & 0 & 0 & \ddots\end{bmatrix}\begin{Bmatrix}x_1\\ x_2\\ x_3\\ \vdots\end{Bmatrix}+\begin{bmatrix}B_1 & 0 & 0 & 0\\ 0 & B_2 & 0 & 0\\ 0 & 0 & B_3 & 0\\ 0 & 0 & 0 & \ddots\end{bmatrix}\begin{Bmatrix}i_{cell(1)}\\ i_{cell(2)}\\ i_{cell(3)}\\ \vdots\end{Bmatrix} \tag{7}$$

$$\begin{Bmatrix}i_1\\ i_2\\ i_3\\ \vdots\\ i_4\end{Bmatrix}=[R]^{-1}([E]\{x\}+[F]I_{cell}+[OCV]\{V_{oc}\}) \tag{8}$$

$$[R]=\begin{bmatrix}1 & 0 & 0 & 0\\ 0 & (-2R_c-R_{o(2)}-R_{o(1)}) & R_{o(2)} & 0\\ 0 & R_{o(2)} & (-2R_c-R_{o(3)}-R_{o(2)}) & R_{o(3)}\\ 0 & \ddots & \ddots & \vdots\end{bmatrix} \tag{9}$$

$$[E]=\begin{bmatrix}0 & 0 & 0 & 0 & 0 & 0 & 0 & 0\\ -1 & -1 & 1 & 1 & 0 & 0 & 0 & 0\\ 0 & 0 & -1 & -1 & 1 & 1 & 0 & 0\\ 0 & 0 & 0 & 0 & -1 & -1 & 1 & 1\end{bmatrix} \tag{10}$$

$$[F]=\begin{Bmatrix}1\\ (-R_{o(1)}+2R_c)\\ 0\\ \vdots\\ 0\end{Bmatrix} \tag{11}$$

$$[OCV]=\begin{bmatrix}1 & 0 & 0 & 0\\ -1 & 1 & 0 & 0\\ 0 & -1 & 1 & 0\\ 0 & 0 & -1 & 1\end{bmatrix}\ (first\ 4\ rows) \tag{12}$$

$$[G]=\begin{bmatrix}1 & -1 & 0 & 0 & 0\\ 0 & 1 & -1 & 0 & 0\\ 0 & 0 & 1 & -1 & 0\\ 0 & 0 & 0 & 1 & -1\end{bmatrix}\ (first\ 4\ rows) \tag{13}$$

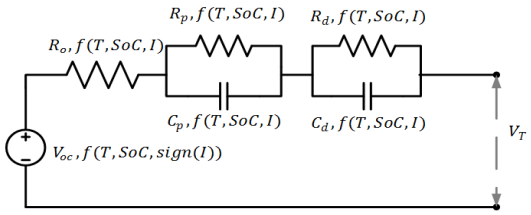

Fig. 5 Equivalent Circuit Approach used for each node

Electrical Model Parameter Definition

As the electrical model relies on accurate data, a strategy needed to be constructed for map population. A pulse testing strategy, similar to [28] and [31] was implemented, with tests being performed at several different temperatures and current magnitudes to give the required data. This used an approach similar to [31], using exponential decay relations in (14) and (15). The data for each resistance parameter was then formed into maps, using an adapted version of the scatteredIntepolant() approach available in MATLAB. OCV and capacity data was also acquired from these tests.

$$V_p=\left(1-e^{\frac{-t}{R_pC_p}}\right)IR_p \tag{14}$$

$$V_d=\left(1-e^{\frac{-t}{R_dC_d}}\right)IR_d \tag{15}$$

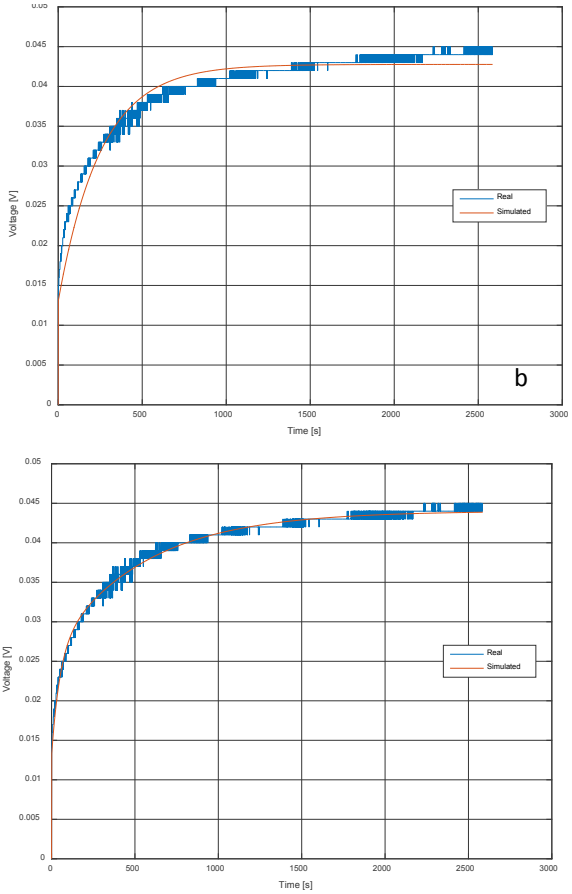

Fig. 6 Fitting of example test data with (a) 1 RC curve, and (b) 2 RC curves

V. Verification of Model

Fig. 7 Cell Thermocouple Test Setup

The model was verified by correlating to experimental data from tests performed on a 28Ah PHEV2 format NMC/graphite lithium-ion cell. The tests performed were a 3C discharge and a Federal Urban Driving Schedule (FUDS) [35], both between 85% and 15% SoC. Both tests were performed with ambient temperature monitoring, but with no active temperature control, and the cell exposed to ambient air. PT100 temperature monitoring was used with an accuracy of 0.1°C, with voltage and current accuracy of approximately 1mV and 0.01A respectively, and measurement timesteps of 100ms. PT100s were placed in 3 positions on the body of the cell, and on each terminal, as shown in Fig. 7. The correlation results are shown in Fig. 8 and Fig. 9, which show temperature comparison against the experimental data for the mid-height body and terminal sensors. The model boundary conditions were considering the cell exposed to ambient air, mimicking the test condition.

For the 3C discharge, the temperature results are within 1.2 ºC. The voltage error is within 10mV underload, and 18mV at the worst point (directly after load is removed). The profile also follows the experimental data well. For the FUDS, the temperature results are within 2.1 ºC, and the worst case voltage error was 40mV. The larger disparity is a function of the high periods of heat generation and due to the more dynamic nature of current application. The results are sufficiently accurate for most applications, but areas of improving accuracy would be to refine the resolution and accuracy of the underlying test data. In particular, a timestep resolution of 100ms made isolating ohmic resistance from dynamic influences difficult, and the voltage accuracy inhibited representative entropic coefficient maps.

Fig. 10 shows the temperature and SoC distribution across the cell when ran with 7 nodes. It is clear that there is some temperature distribution in the regions of high current, but the internal conduction leads this to be resolved again in periods of relaxation. Because of the relatively mild and short duration of temperature distribution, the effect on cell lithiation distribution is low, and the cell maintains a largely homogeneous state. This is due to the periods of low or no current in the FUDS cycle allowing the cell to balance thermal and electrical characteristics. Testing under conditions of prolonged high current, or on higher capacity, energy dense cells would allow for greater analysis of thermal/electrical cell heterogeneity.

VI. Conclusions and Further Work

A 1D electrical and thermal closed loop cell model was developed. The model was developed, using the Matlab/Simulink platform, in order to be applicable to a range of cell chemistries and geometries as well as be compact and fast calculating. The underlying equations were presented and described. The model was verified both under constant current and dynamic conditions. The model accurately estimates cell voltage and temperature response to current application, even under dynamic drive cycles. The model also emulates thermal and electrical distributions to a high degree of accuracy, although the capability of the test cell to maintain even conditions did not allow this to be fully evaluated. To further develop this model, testing should be done on a larger, more energy orientated cell to see the results.

A. Acknowledgment

I would like to thank Horiba-MIRA for their support, funding, and provision of simulation and testing capability.

B. Nomenclature

I	Cell Current [A]
R_p	Charge Transfer Polarization Resistance [Ohm]
R_d	Diffusion Resistance [Ohm]
R_o	Ohmic Resistance [Ohm]
R_c	Connection Resistance [Ohm]
C_p	Charge Transfer Polarization Capacitance [Farad]

C_d	Diffusion Capacitance [Farad]
V_p	Charge Transfer Polarization Voltage [V]
V_d	Diffusion Voltage [V]
V_{oc}	Open Circuit Voltage [V]
V_T	Terminal Voltage [V]
Cp_{cell}	Cell specific heat capacity [J/kgK]
T	Temperature [K]
m_{cell}	Cell mass [kg]
h_s	Cell convection coefficient [W/ m²]
A_s	Cell surface area [m²]

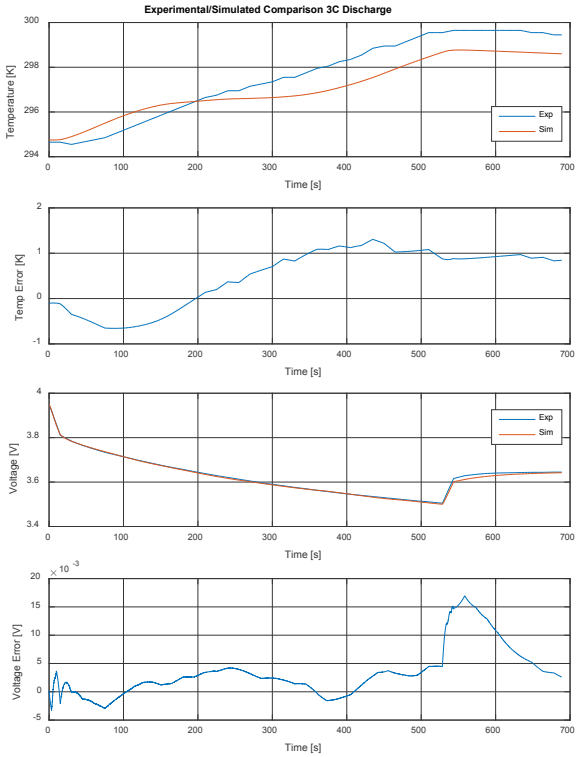

Fig. 8 3C Discharge correlation between experimental and simulation data

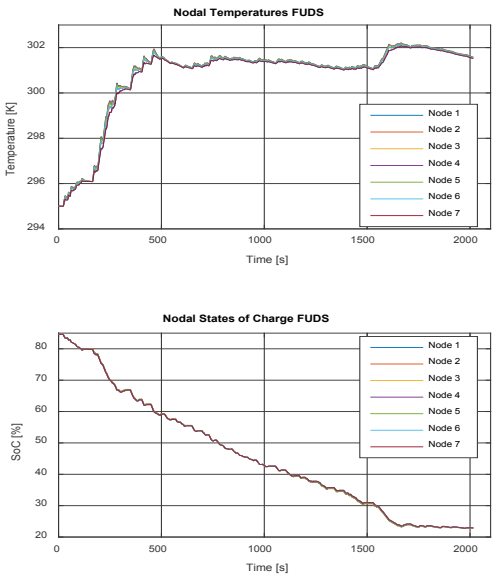

Fig. 9 Nodal temperature and SoC evolution through FUDS.

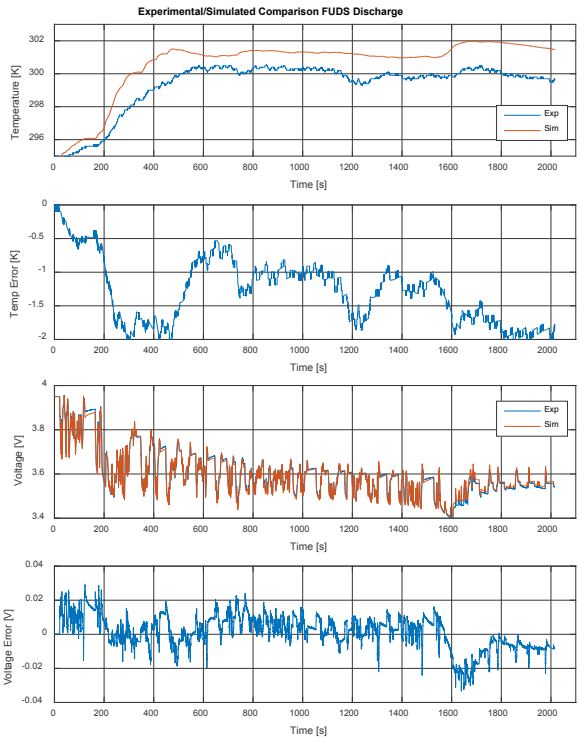

Fig. 10 Comparison of Experimental and Simulated Data FUDS

REFERENCES

[1] P. Cazzola, M. Gorner, and L. Munuera, "Global EV Outlook 2017: Two million and counting," 2017.

[2] M. S. Rad, D. L. Danilov, M. Baghalha, M. Kazemeini, P. H. L. Notten, and E. T. Al, "Thermal Modeling of Cylindrical LiFePO 4 Batteries," vol. 2013, no. July, pp. 1–7, 2013.

[3] R. Zhao, J. Liu, and J. Gu, "The effects of electrode thickness on the electrochemical and thermal characteristics of lithium ion battery," *Appl. Energy*, vol. 139, pp. 220–229, 2015.

[4] S. Panchal, I. Dincer, M. Agelin-chaab, R. Fraser, and M. Fowler, "Experimental and theoretical investigation of temperature distributions in a prismatic lithium-ion battery," *Int. J. Therm. Sci.*, vol. 99, pp. 204–212, 2016.

[5] W. Dhammika, P. A. A. Paul, D. Worwood, E. Hosseinzadeh, Q. Kellner, J. Marco, D. Greenwood, and R. Mcglen, "Thermal analysis of a lithium-ion pouch cell under aggressive automotive duty cycles with minimal cooling," in *IET Hybrid Electric Vehicle Conference*, 2016, pp. 2–3.

[6] Y. Troxler, B. Wu, M. Marinescu, V. Yufit, Y. Patel, A. J. Marquis, N. P. Brandon, and G. J. Offer, "The effect of thermal gradients on the performance of lithium-ion batteries," *J. Power Sources*, vol. 247, pp. 1018–1025, 2014.

[7] J. Jaguemont, L. Boulon, P. Venet, Y. Dube, and A. Sari, "Lithium Ion Battery Aging Experiments at Sub-Zero Temperatures and Model Development for Capacity Fade Estimation," *IEEE Trans. Veh. Technol.*, vol. 9545, no. c, pp. 1–1, 2015.

[8] V. Sangwan, A. Sharma, R. Kumar, and A. K. Rathore, "Equivalent

circuit model parameters estimation of Li-ion battery: C-rate, SOC and temperature effects," *2016 IEEE Int. Conf. Power Electron. Drives Energy Syst.*, pp. 1–6, 2016.

[9] X. Hu, S. Li, and H. Peng, "A comparative study of equivalent circuit models for Li-ion batteries," *J. Power Sources*, vol. 198, pp. 359–367, 2012.

[10] T. M. Bandhauer, S. Garimella, and T. F. Fuller, "A Critical Review of Thermal Issues in Lithium-Ion Batteries," *J. Electrochem. Soc.*, 2011.

[11] T. Waldmann, M. Wilka, M. Kasper, M. Fleischhammer, and M. Wohlfahrt-Mehrens, "Temperature dependent ageing mechanisms in Lithium-ion batteries - A Post-Mortem study," *J. Power Sources*, vol. 262, pp. 129–135, 2014.

[12] D. Anseán, M. González, J. C. Viera, J. C. Álvarez, C. Blanco, and V. M. García, "Electric Vehicle Li-ion Battery Evaluation based on Internal Resistance Analysis," in *Vehicle Power and Propulsion Conference (VPPC)*, 2014, pp. 0–5.

[13] A. Tourani, "Investigation into operating temperature effect on the performance of high capacity lithium-ion cells," 2013.

[14] I. A. Hunt, Y. Zhao, Y. Patel, and G. J. Offer, "Surface Cooling Causes Accelerated Degradation Compared to Tab Cooling for Lithium-Ion Pouch Cells," *J. Electrochem. Soc.*, vol. 163, no. 9, pp. 1846–1852, 2016.

[15] M. Marinescu, B. Wu, M. Von Srbik, V. Yufit, and G. J. Offer, "The effect of thermal gradients on the performance of battery packs in automotive applications," in *Hybrid and Electric Vehicles Conference, IET*, 2013, pp. 1–5.

[16] A. Samba, "Battery Electrical Vehicles-Analysis of Thermal Modelling and Thermal Management," LUSAC (Laboratoire Universitaire des Sciences Appliqu´ ees de Cherbourg), Universit´ e de caen Basse Normandie, 2016.

[17] S. Chacko and Y. M. Chung, "Thermal modelling of Li-ion polymer battery for electric vehicle drive cycles," *J. Power Sources*, vol. 213, pp. 296–303, 2012.

[18] J. Jaguemont, L. Boulon, and Y. Dubé, "A comprehensive review of lithium-ion batteries used in hybrid and electric vehicles at cold temperatures," *Appl. Energy*, vol. 164, pp. 99–114, 2016.

[19] S. Bazinski and X. Wang, "Determining Entropic Coefficient of the LFP Prismatic Cell at Various Temperatures and Charge/Discharge States," *ECS Trans.*, vol. 45, no. 29, pp. 85–92, 2013.

[20] Z. Rao and S. Wang, "A review of power battery thermal energy management," *Renew. Sustain. Energy Rev.*, vol. 15, no. 9, pp. 4554–4571, 2011.

[21] F. Savoye, P. Venet, M. Millet, and J. Groot, "Impact of periodic current pulses on Li-ion battery performance," *IEEE Trans. Ind. Electron.*, vol. 59, no. SEPTEMBER 2012, pp. 3481–3488, 2012.

[22] S. Kawano, F. Nishimura, K. Kaprans, G. Bajars, X. Xie, J. Zhu, H. Zhou, D. Gradiometer, S. Tanaka, T. Akai, A. A. Arie, and J. K. Lee, "Simplified Heat Generation Model for Lithium ion battery used in Electric Vehicle."

[23] G. F. . Rogers and Y. . Mayhew, *Thermodynamic and Transport Properties of Fluids*, 5th ed. Oxford: Blackwell Publishing, 2010.

[24] S. W.Churchill and H. H.S.Chu, "Correlating equations for laminar and turbulent free convection from a vertical plate," *Int. J. Heat Mass Transf.*, vol. 18, no. 11, pp. 1323–1329, 1975.

[25] S. W.Churchill and H. H.S.Chu, "Correlating equations for laminar and turbulent free convection from a horizontal cylinder," *Int. J. Heat Mass Transf.*, vol. 18, no. 9, pp. 1049–1053, 1975.

[26] L. H. Saw, Y. Ye, and A. A. O. Tay, "Electro-thermal analysis and integration issues of lithium ion battery for electric vehicles," vol. 131, pp. 97–107, 2014.

[27] W. Waag, S. Käbitz, and D. U. Sauer, "Experimental investigation of the lithium-ion battery impedance characteristic at various conditions and aging states and its influence on the application," *Appl. Energy*, vol. 102, pp. 885–897, 2013.

[28] C. W. E. Fok, "Simulation of Lithium-Ion Batteries Based on Pulsed Current Characterization," The University of British Colombia, 2016.

[29] C. R. Birkl, E. McTurk, M. R. Roberts, P. G. Bruce, and D. A. Howey, "A Parametric Open Circuit Voltage Model for Lithium Ion Batteries," *J. Electrochem. Soc.*, vol. 162, no. 12, pp. A2271–A2280, 2015.

[30] L. Pei, T. Wang, R. Lu, and C. Zhu, "Development of a voltage relaxation model for rapid open-circuit voltage prediction in lithium-ion batteries," *J. Power Sources*, vol. 253, pp. 412–418, 2014.

[31] C. Wu, R. Fu, Z. Xu, and Y. Chen, "Improved State of Charge Estimation for High Power Lithium Ion Batteries Considering Current Dependence of Internal Resistance," *Energies*, vol. 10, no. 10, p. 1486, 2017.

[32] J. Zhang and J. Lee, "A review on prognostics and health monitoring of Li-ion battery," *J. Power Sources*, vol. 196, no. 15, pp. 6007–6014, 2011.

[33] Y. Zhou and X. Li, "Overview of lithium-ion battery SOC estimation," *2015 IEEE Int. Conf. Inf. Autom. ICIA 2015 - conjunction with 2015 IEEE Int. Conf. Autom. Logist.*, no. August, pp. 2454–2459, 2015.

[34] T. Bruen and J. Marco, "Modelling and experimental evaluation of parallel connected lithium ion cells for an electric vehicle battery system," *J. Power Sources*, vol. 137, pp. 511–536, 2015.

[35] USABC, "Electric Vehicle Battery Test Procedures Manual Revision 2," 1996.